AIAA 80-1443R

Determination of Three-Dimensional Flow Separation by a Streamline Method

Tsze C. Tai*
David Taylor Naval Ship Research and Development Center, Bethesda, Md.

A streamline approach for determining the free vortex-layer type, three-dimensional flow separation is presented. The procedure is based on the Maskell postulation about separation patterns in three dimensions. The line of separation is determined by the envelope of converging streamlines inside the viscous layer. The required streamlines are calculated by three ordinary differential equations, using inviscid pressures along with proper viscous damping parameters. The method is illustrated by two examples, a prolate spheroid in an incompressible flow and a spherically blunted cone at hypersonic speed, both at moderate angles of attack. Comparisons of the theoretical results with experiments and a three-dimensional boundary-layer solution are made.

Nomenclature

a,b	= major and minor axes of an ellipsoid
e	= eccentricity
f	= local body radial distance from the centerline
g_{ij},g^{ij}	= metric tensor for body geometry
h_1,h_2	= metric coefficients for coordinates ξ,β
ℓ	= length of a body
M	= Mach number
P	= static pressure
R	= nose radius
S	= distance along a streamline measured from the stagnation point
u,v,w	= velocity components in body-oriented coordinates
V	= velocity
x,ϕ,z	= body-oriented nonorthogonal coordinates
$\bar{x},\bar{y},\bar{z}$	= Cartesian coordinates
α	= angle of attack
γ	= ratio of specific heats
θ	= streamline angle
λ	= coefficient for friction model
μ	= viscosity
ξ,β,ζ	= streamwise coordinates
ρ	= density
$-\rho\overline{u'w'},-\rho\overline{v'w'}$	= Reynolds stresses
τ	= shearing stress

Subscripts

i	= initial condition
0	= stagnation
1,2	= x, ϕ direction
∞	= freestream

Introduction

THE criterion for flow separation in three dimensions is radically different from the conventional concept based on two-dimensional flows, where separation takes place as the skin friction vanishes. In three-dimensional flows, the vanishing of skin friction in either or both directions cannot be used to define a flow separation. Instead, the concept of the envelope of limiting streamlines as the separation line has been developed. First suggested by Eichelbrenner and Oudart,[1] the envelope idea was further explored by Maskell,[2] based on general flow observations, and supported by Wang[3] from the standpoint of numerical results. A comprehensive review of the subject was given by Wang.[4]

Maskell[2] postulated two basic forms of separation patterns in three dimensions: a bubble and a free vortex (or shear) layer. In the case of a bubble, the surface of separation encloses fluid which is not part of the mainstream but is carried along with the body surface. In the case of a vortex layer, both sides of the separation surface are filled with the main stream fluid. Although each displays a different flow structure, the line of separation is generally identified as an envelope of the limiting streamlines. In reality, a combination of both types of flow separation with a bubble and a free vortex layer is most likely to exist.

The Maskell descriptions, which are representations of experimental observations, are found by Wang[4] to be consistent with the three-dimensional boundary-layer theory. Wang[4] introduced an open and close separation concept, however. In a closed separation, the separated region is inaccessible to the upstream flow. For an open separation, on the other hand, the limiting streamlines on both sides of the separation line stem from the same front stagnation point; the separated region is accessible to the upstream flow. Physically, therefore, Wang's closed-type separation corresponds to Maskell's bubble type, and the open-type separation corresponds to the vortex-layer type. The open separation concept, which is relatively new, has been substantiated by recent measurements made by Kreplin et al.[5] and Han and Patel.[6]

Formation of Vortex-Layer-Type Separation

Of particular importance is the vortex-layer-type separation (or the open type) which covers a wide class of flows of practical interest. Flows around a body of revolution at angles of attack that often model spacecraft,[7] missiles,[8] and other similar configurations[9] in maneuver, fall into this category. Also, free vortices over a wing-body combination[10] or in a ship stern[11] are generated by the vortex-layer-type separation due to convergence of streamlines which originated from a common upstream flow. The phenomenon is unique in three-dimensional flows.

Maskell's postulation on the free vortex-layer-type separation pattern is shown in Fig. 1, which is based on description given in Ref. 12. It is noted that above the limiting streamlines, there lie the inviscid streamlines. Since the limiting streamlines and the inviscid streamlines are both influenced by the surface pressure distribution and the

Presented as Paper 80-1443 at the AIAA 13th Fluid and Plasma Dynamics Conference, Snowmass, Colo., July 14-16, 1980; submitted Sept. 24, 1980; revision received Feb. 18, 1981.

*Research Aerospace Engineer, Aviation and Surface Effects Department. Member AIAA.

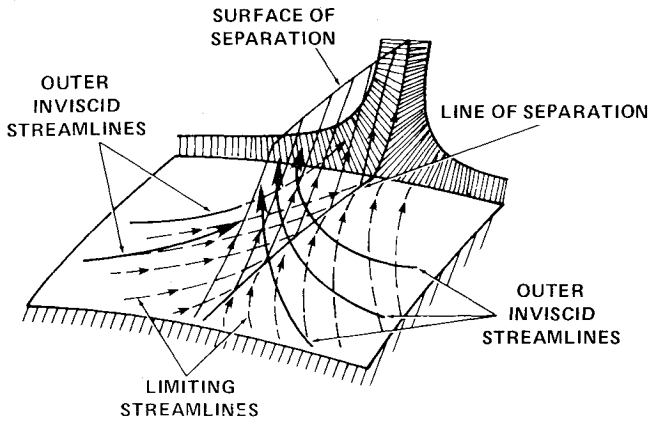

Fig. 1 Maskell's postulation on three-dimensional flow separation forming a free vortex layer.

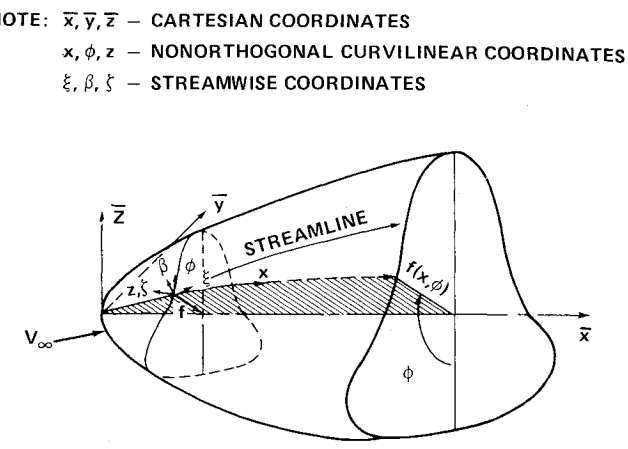

Fig. 2 Coordinate systems for a general three-dimensional body.

deviation between the two is strictly a boundary-layer phenomenon, it is proper to suggest that the limiting streamlines are eventually dictated by the streamlines above them. The line of separation, which is an envelope of the limiting streamlines, therefore, can be determined approximately by the loci of converging streamlines inside or at the edge of the boundary layer. These streamlines, however, must be calculated accurately based on realistic pressure distributions containing physical properties that have direct bearing on the flow behavior. Experimental or empirical pressure distributions or theoretical pressures obtained by means of viscous-inviscid interactions involving not only attached flow but also separation are considered to possess such physical properties. If pure inviscid pressures are used, proper viscous damping terms should be incorporated to stimulate the real flow.

In the present analysis, a method is developed to determine the vortex-layer-type separation by the envelope of converging streamlines inside or at the edge of the boundary layer. An exact, yet simple method for determining the inviscid streamline geometry over general three-dimensional bodies has been developed. To trace the streamlines inside the boundary layer, the method is extended to viscous flows by adding a friction model. The latter is particularly useful when realistic pressure distribution is not available.

Inviscid Streamline Equations

General Three-Dimensional Body

Few analyses have been developed in the literature to obtain the inviscid streamline geometry.[13-16] Here we will consider an exact method using nonorthogonal systems. In body-oriented nonorthogonal coordiantes (x,ϕ,z), the inviscid momentum equations for the flow over the surface of a general three-dimensional body can be written as follows.[17]

x–Momentum

$$u\frac{\partial u}{\partial x}+\frac{v}{g_{22}^{1/2}}\frac{\partial u}{\partial \phi}+\left(\frac{uvg^{12}}{g_{22}^{1/2}}-\frac{v^2g^{11}}{2g_{22}}\right)\frac{\partial g_{22}}{\partial x}+\frac{v^2g^{12}}{2g_{22}}\frac{\partial g_{22}}{\partial \phi}$$
$$+u^2g^{12}\frac{\partial g_{12}}{\partial x}+\frac{v^2g^{11}}{g_{22}}\frac{\partial g_{12}}{\partial \phi}=-\frac{1}{\rho}g^{11}\frac{\partial P}{\partial x}+g^{12}\frac{\partial P}{\partial \phi} \tag{1}$$

ϕ–Momentum

$$u\frac{\partial v}{\partial x}+\frac{v}{g_{22}^{1/2}}\frac{\partial v}{\partial \phi}+\left[uv\left(g^{22}-\frac{1}{2g_{22}}\right)-\frac{v^2g^{12}}{2g_{22}^{1/2}}\right]\frac{\partial g_{22}}{\partial x}$$
$$+\frac{v^2}{2g_{22}^{1/2}}\left(g^{22}-\frac{1}{g_{22}}\right)\frac{\partial g_{22}}{\partial \phi}+u^2g_{22}^{1/2}g^{22}\frac{\partial g_{12}}{\partial x}+\frac{v^2g^{12}}{g_{22}^{1/2}}\frac{\partial g_{12}}{\partial \phi}$$
$$=-\frac{g_{22}}{\rho}\left(g^{12}\frac{\partial P}{\partial x}+g^{22}\frac{\partial P}{\partial \phi}\right) \tag{2}$$

where x is the distance along the body surface of a constant ϕ plane, ϕ the azimuthal angle measured from the most windward line, and z normal to the surface (see Fig. 2). The velocity components u and v are measured along the surface in x and ϕ directions, respectively, and P and ρ are the static pressure and density, respectively. The g_{ij} is the metric tensor for the body geometry and g^{ij} is the conjugate metric tensor of g_{ij}. Their expressions are given in Ref. 17.

The geometry of any streamline emanating from the stagnation point may be expressed as $\phi=\phi\ (x,\beta)$, where β is constant along a stramline. The coordinates are related to the velocity components through the relation, with the aid of the following sketch.

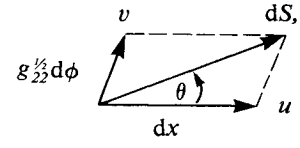

$$u:dx=v:g_{22}^{1/2}d\phi \qquad \frac{g_{22}^{1/2}d\phi}{dx}=\frac{v}{u} \tag{3}$$

Defining D/Dx as the substantial derivative, or derivative along a streamline, Eq. (3) can be written in the form

$$\frac{D\phi}{Dx}=\frac{v}{g_{22}^{1/2}u} \tag{4}$$

Differentiate the preceding equation with respect to x to get

$$\frac{D^2\phi}{Dx^2}=\frac{1}{g_{22}^{1/2}}\left[\frac{u\dfrac{Dv}{Dx}-v\dfrac{Du}{Dx}}{u^2}-\frac{v}{2u}\frac{1}{g_{22}}\frac{Dg_{22}}{Dx}\right] \tag{5}$$

Also, introduce a variable θ, the angle between the tangent of local streamline and the x axis by the relation

$$\theta=\arccos\left[\frac{1+g_{12}\dfrac{D\phi}{Dx}}{\sqrt{1+2g_{12}\dfrac{D\phi}{Dx}+g_{22}\left(\dfrac{D\phi}{Dx}\right)^2}}\right] \tag{6}$$

Differentiating Eq. (6) with respect to x along a streamline and rearranging, yields

$$\frac{D^2\phi}{Dx^2}=\frac{\sin\theta\,[1+2g_{12}t+g_{22}t^2]^{3/2}\dfrac{D\theta}{Dx}}{(g_{22}-g_{12}^2)t}$$
$$-\frac{\left[(1+g_{12}t)\dfrac{Dg_{22}}{Dx}-2(g_{12}+g_{22}t)\dfrac{Dg_{12}}{Dx}\right]t}{2(g_{22}-g_{12}^2)t} \tag{7}$$

where $t = D\phi/Dx$. Equating Eqs. (5) and (7), yields

$$\frac{D\theta}{Dx} = F\left(x,\phi,u,v,\frac{Du}{Dx},\frac{Dv}{Dx}\right) \tag{8}$$

Integration of Eq. (8) gives the local direction of a streamline. For streamlines in the nose region that first move forward from the stagnation point and then bend toward the leeside, the Dx term experiences zero movement adjacent to the turning point. It causes the derivative to approach infinity. To amend such a numerical problem, the length of the streamline S is used as the independent variable instead of x. Accordingly, Eq. (8) is recast in the form

$$\frac{D\theta}{DS} = \frac{D\theta}{Dx}\frac{Dx}{DS} = \frac{Dx}{DS}F\left(x,\phi,u,v,\frac{Du}{Dx},\frac{Dv}{Dx}\right) \tag{9}$$

The expressions for the total derivatives Du/Dx and Dv/Dx in Eq. (9) are obtained from Eqs. (1) and (2) in conjunction with the following relations:

$$\frac{Du}{Dx} = \frac{\partial u}{\partial x}\frac{Dx}{Dx} + \frac{\partial u}{\partial \phi}\frac{D\phi}{Dx} = \frac{\partial u}{\partial x} + \frac{v}{ug_{22}^{1/2}}\frac{\partial u}{\partial \phi} \tag{10}$$

Rearranging Eq. (1) and substituting in Eq. (10), there results

$$\frac{Du}{Dx} = -\left(\frac{vg^{12}}{g_{22}^{1/2}} - \frac{v^2g^{11}}{2ug_{22}}\right)\frac{\partial g_{22}}{\partial x} - \frac{v^2g^{12}}{2ug_{22}}\frac{\partial g_{22}}{\partial \phi}$$
$$- ug^{12}\frac{\partial g_{12}}{\partial x} - \frac{v^2g^{11}}{ug_{22}}\frac{\partial g_{12}}{\partial \phi} - \frac{1}{\rho u}\left(g^{11}\frac{\partial P}{\partial x} + g^{12}\frac{\partial P}{\partial \phi}\right) \tag{11}$$

In a similar manner, Eq. (2) gives

$$\frac{Dv}{Dx} = \frac{\partial v}{\partial x} + \frac{v}{ug_{22}^{1/2}}\frac{\partial v}{\partial \phi} = -\left[v\left(g^{22} - \frac{1}{2g_{22}}\right) - \frac{v^2g^{12}}{2ug_{22}^{1/2}}\right]\frac{\partial g_{22}}{\partial x}$$
$$- \frac{v^2}{2ug_{22}^{1/2}}\left(g^{22} - \frac{1}{g_{22}}\right)\frac{\partial g_{22}}{\partial \phi} - ug_{22}^{1/2}g^{22}\frac{\partial g_{12}}{\partial x} - \frac{v^2g^{12}}{ug_{22}^{1/2}}\frac{\partial g_{12}}{\partial \phi}$$
$$- \frac{g_{22}^{1/2}}{\rho u}\left(g^{12}\frac{\partial P}{\partial x} + g^{22}\frac{\partial P}{\partial \phi}\right) \tag{12}$$

Furthermore, that

$$\frac{v}{u} = g_{22}^{1/2}\frac{D\phi}{Dx} \qquad \text{bis} \quad (4)$$

and

$$u^2 = \frac{\gamma M^2 P}{\rho}\left\{1\Big/\left[1 + 2g_{12}\frac{D\phi}{Dx} + g_{22}\left(\frac{D\phi}{Dx}\right)^2\right]\right\} \tag{13}$$

Using Eqs. (11-13), Eq. (9) can be completed to read

$$\frac{D\theta}{DS} = \frac{1}{\sqrt{(\epsilon^2 + 2g_{12}\epsilon\sigma + g_{22}\sigma^2)(g_{22} - g_{12}^2)}}$$
$$\times\left\{\frac{1}{\gamma M^2 P}\left[(g_{12}\epsilon + g_{22}\sigma)\frac{\partial P}{\partial x} - (\epsilon + g_{12}\sigma)\frac{\partial P}{\partial \phi}\right]\right.$$
$$\left. - \frac{\sigma}{2}\frac{\partial g_{22}}{\partial x} - \epsilon\frac{\partial g_{12}}{\partial x}\right\} \tag{14}$$

The geometrical relations between the x and S, and ϕ and S are

$$\frac{Dx}{DS} = \frac{\epsilon}{\sqrt{\epsilon^2 + 2g_{12}\sigma\epsilon + g_{22}\sigma^2}} \tag{15}$$

$$\frac{D\phi}{DS} = \frac{\sigma}{\sqrt{\epsilon^2 + 2g_{12}\sigma\epsilon + g_{22}\sigma^2}} \tag{16}$$

where

$$\epsilon = g_{22}\cos^2\theta - g_{12}^2 \tag{17}$$

$$\sigma = g_{12}\sin^2\theta + (g_{22} - g_{12}^2)^{1/2}\sin\theta\cos\theta \tag{18}$$

Equations (14-16) constitute a set of first-order, ordinary differential equations for determining the geometry of a chosen streamline from the known pressure distribution. The method is considered exact in the sense that no approximations have been made in the process of derivation and provided that exact expressions for the pressure gradients can be incorporated. The streamline pattern so calculated will depend strongly upon the input pressure distribution. The more realistic is the input pressure distribution, the more realistic is the streamline geometry, including the streamline convergence for determining the three-dimensional flow separation to be further discussed later.

Body of Revolution at Incidence

For a body of revolution at incidence, where the x and ϕ coordinates can be set orthogonal, simplification can be achieved by letting

$$\left.\begin{aligned} g_{12} &= \frac{\partial g_{12}}{\partial x} = \frac{\partial g_{12}}{\partial \phi} = \frac{\partial g_{22}}{\partial \phi} = 0 \\ g_{22} &= f^2 \end{aligned}\right\} \text{ orthogonal system only}$$

Equations (1) and (2) are reduced to the following form

x – Momentum (orthogonal system only)

$$u\frac{\partial u}{\partial x} + \frac{v}{f}\frac{\partial u}{\partial \phi} - \frac{v^2}{f}\frac{df}{dx} = -\frac{1}{\rho}\frac{\partial P}{\partial x} \tag{19}$$

ϕ – Momentum (orthogonal system only)

$$u\frac{\partial v}{\partial x} + \frac{v}{f}\frac{\partial v}{\partial \phi} + \frac{uv}{f}\frac{df}{dx} = -\frac{1}{\rho f}\frac{\partial P}{\partial \phi} \tag{20}$$

Following the same procedure, Eqs. (19) and (20) can be reduced to ordinary forms for calculating the streamline geometry of a body of revolution at incidence

$$\left(\frac{D\theta}{DS}\right)_{orth} = \frac{1}{\gamma M^2 P}\left(\frac{\partial P}{\partial x}\sin\theta - \frac{1}{f}\frac{\partial P}{\partial \phi}\cos\theta\right) - \frac{1}{f}\frac{df}{dx}\sin\theta \tag{21}$$

$$\left(\frac{D\phi}{DS}\right)_{orth} = \frac{\sin\theta}{f} \tag{22}$$

$$\left(\frac{Dx}{DS}\right)_{orth} = \cos\theta \tag{23}$$

Streamlines Inside a Boundary Layer

Equations for Viscous Streamlines

Many times a realistic pressure distribution is not available. To simulate the physical flow, so that the flow separation can be detected, it is necessary to consider streamlines inside the boundary layer; see Fig. 3. Without losing generality, a body of revolution at incidence will be considered as an illustration.

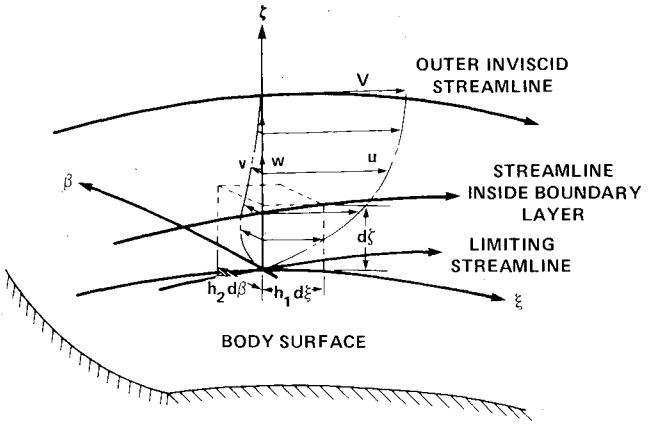

Fig. 3 Streamlines in a boundary layer.

The equations of motion that govern a three-dimensional boundary-layer flow can be written as follows.

x-Momentum

$$u\frac{\partial u}{\partial x}+\frac{v}{f}\frac{\partial u}{\partial \phi}+w\frac{\partial u}{\partial z}-\frac{v^2}{f}\frac{df}{dx}=-\frac{1}{\rho}\left(\frac{\partial P}{\partial x}-\frac{\partial \tau_1}{\partial z}\right) \tag{24}$$

ϕ-Momentum

$$u\frac{\partial v}{\partial x}+\frac{v}{f}\frac{\partial v}{\partial \phi}+w\frac{\partial v}{\partial z}+\frac{uv}{f}\frac{df}{dx}=-\frac{1}{\rho}\left(\frac{1}{f}\frac{\partial P}{\partial \phi}-\frac{\partial \tau_2}{\partial z}\right) \tag{25}$$

where τ_1 and τ_2 are the shearing stresses in x and ϕ directions, respectively, i.e.,

$$\tau_1=\mu\frac{\partial u}{\partial z}-\rho\overline{u'w'} \tag{26}$$

$$\tau_2=\mu\frac{\partial v}{\partial z}-\rho\overline{v'w'} \tag{27}$$

The substantial derivatives along a streamline inside a three-dimensional boundary layer are

$$\frac{Du}{Dx}=\frac{\partial u}{\partial x}+\frac{v}{uf}\frac{\partial u}{\partial \phi}+\frac{w}{u}\frac{\partial u}{\partial z} \tag{28}$$

$$\frac{Dv}{Dx}=\frac{\partial v}{\partial x}+\frac{v}{uf}\frac{\partial v}{\partial \phi}+\frac{w}{u}\frac{\partial v}{\partial z} \tag{29}$$

It indicates that additional z-component terms in Eqs. (24) and (25) can be absorbed in the total derivatives in the derivation of the streamline equations. Following the same procedure as for the inviscid case, the resulting ordinary equations for calculating the streamline geometry inside a boundary layer are

$$\left(\frac{D\theta}{DS}\right)_{\text{viscous}}=\frac{1}{\gamma M^2 P}\left[\left(\frac{\partial P}{\partial x}-\frac{\partial \tau_1}{\partial z}\right)\sin\theta-\left(\frac{1}{f}\frac{\partial P}{\partial \phi}-\frac{\partial \tau_2}{\partial z}\right)\cos\theta\right]-\frac{1}{f}\frac{df}{dx}\sin\theta \tag{30}$$

$$\left(\frac{D\phi}{DS}\right)_{\text{viscous}}=\frac{\sin\theta}{f} \tag{31}$$

$$\left(\frac{Dx}{DS}\right)_{\text{viscous}}=\cos\theta \tag{32}$$

Note that terms in parentheses in Eq. (30) represent the effective pressure gradients for computing θ.

Friction Model

The addition of friction terms $\partial\tau_1/\partial z$ and $\partial\tau_2/\partial z$ makes the system of Eqs. (30-32) not readily solvable even if the pressure values are provided. A proper determination of these terms, of course, is to solve the three-dimensional boundary-layer equations. Even that, the solution involves turbulence modeling which has been a problem for many years. It is attempted, therefore, to model these friction terms without solving the complex three-dimensional boundary-layer problem.

First, consider that in a boundary-layer flow, the frictional force is of comparable order of magnitude with the inertial force. Schlichting[18] suggested that for a flat plate, the friction per unit volume can be estimated by the condition of equality of the frictional and inertial forces

$$\frac{\partial \tau}{\partial z}\sim\frac{\rho V^2}{\ell}\ \text{(for a flat plate)}$$

where ℓ is the characteristic length of the body in question. It is assumed that the flow under consideration is locally similar to that over a flat plate and that other influences can be absorbed in an empirical relation

$$\frac{\partial \tau}{\partial z}=\bar{\lambda}\frac{\rho V^2}{\ell}=\bar{\lambda}\frac{\rho V_\infty^2}{\ell}\left(\frac{V}{V_\infty}\right)^2=\lambda\left(\frac{V}{V_\infty}\right)^2 \tag{33}$$

Then, the component in the x direction can be written as

$$\frac{\partial \tau_1}{\partial z}=\frac{\partial}{\partial z}\left(\mu\frac{\partial u}{\partial z}-\rho\overline{u'w'}\right)=\lambda_1\left(\frac{u}{V_\infty}\right)^2 \tag{34}$$

and that in the ϕ direction

$$\frac{\partial \tau_2}{\partial z}=\frac{\partial}{\partial z}\left(\mu\frac{\partial v}{\partial z}-\rho\overline{v'w'}\right)=\lambda_2\left(\frac{v}{V_\infty}\right)^2 \tag{35}$$

The parameter λ could be a function of Reynolds number, Mach number, pressure gradient, and possibly, the angle of attack. To simplify the approach, it is assumed that λ takes on the following form:

$$\lambda_1=a_1+b_1(\bar{x}/\ell) \tag{36}$$

and

$$\lambda_2=a_2+b_2\phi \tag{37}$$

where a_1, b_1, a_2, and b_2 are constants to be determined empirically and ϕ is in radian. It is noted that near the wall, the sign for λ is affected directly by the velocity profile, which ultimately is dominated by the pressure gradient.[18] These closure statements, which merely represent a working formula, are far from complete. Further improvement might have to be pursued in a similar way for modeling the turbulence in usual boundary-layer computations.

Determination of Three-Dimensional Flow Separation

With the streamline method available, the flow separation can be approximately determined by convergence of streamlines at the edge of or inside the boundary layer, depending on the particular pressure distribution used. If a realistic pressure distribution is available, i.e., experimental or empirical pressure distribution, or theoretical pressures obtained by means of viscous-inviscid interactions, the simple inviscid streamline approach can be employed. For the case of a pure inviscid pressure, then the streamlines must be calculated with proper viscous terms included. The former will be illustrated by the case of a spherically blunted cone at an angle of attack at a hypersonic speed and the latter demonstrated by a prolate spheroid at moderate incidences in an incompressible flow. In both cases, the streamlines are

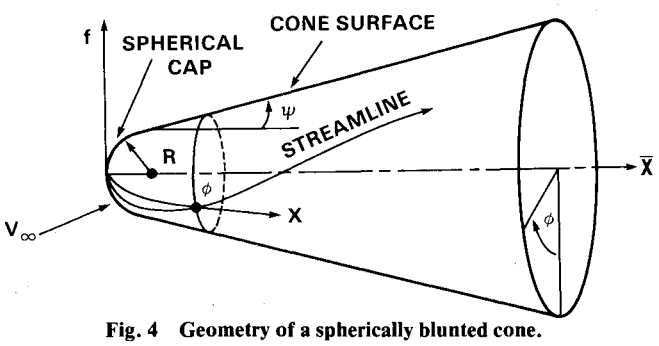

Fig. 4 Geometry of a spherically blunted cone.

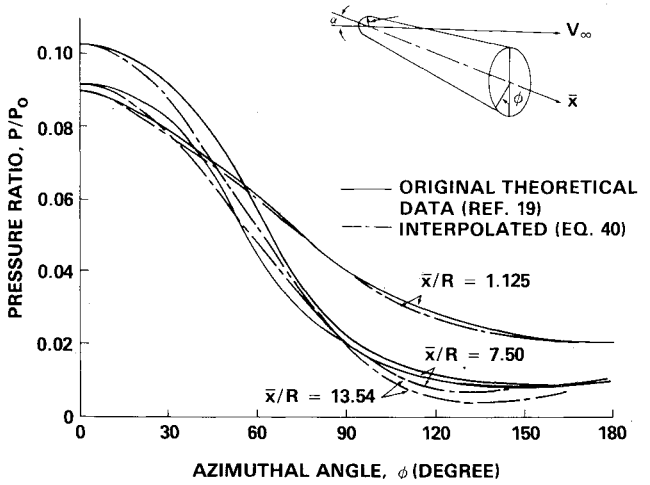

Fig. 5 Pressure distributions over a 9-deg half-angle spherically blunted cone at $M_\infty = 18$ and $\alpha = 10$ deg.

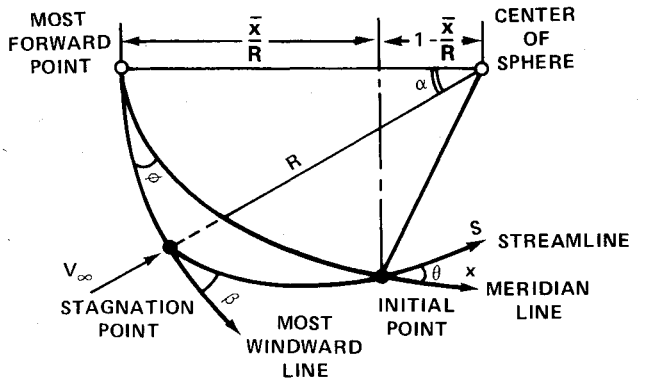

Fig. 6 Initial conditions on a spherical cap.

computed by the initial value technique. That is, all the streamlines originate from the forward stagnation point and the envelope of converging streamlines is traced out by the interception of streamlines from windward and leeward sides. Once two streamlines intercept, it is assumed that they immediately leave the surface, resulting in a flow separation.

Determination of Flow Separation over a Spherically Blunted Cone at Incidence

In hypersonic flows, a typical configuration frequently considered in the past is the spherically blunted cone. Experimental and theoretical pressure distributions for the case of a 9-deg half-angle cone at $M_\infty = 18$ and specific angles of attack were made available by Knox and Lewis.[19] The body geometry can be expressed as follows; see Fig. 4.

For spherical cap:

$$\frac{f}{R} = \sqrt{2\left(\frac{\bar{x}}{R}\right) - \left(\frac{\bar{x}}{R}\right)^2} \tag{38}$$

For the cone:

$$\frac{f}{R} = \sec\psi + \frac{\bar{x} - R}{R}\tan\psi \tag{39}$$

where ψ is the cone half angle.

To obtain the pressure gradients required by the present method, the empirical interpolation formula suggested by Zakkay[20] is employed

$$\frac{P}{P_0} = \left(\frac{P}{P_0}\right)_{\alpha=0} + \bar{A}\alpha\cos\phi + \bar{B}\alpha^2 + \bar{C}\alpha^3\cos 2\phi$$

which can be recast into the form

$$P/P_0 = A\cos\phi + B + C\cos 2\phi \tag{40}$$

where A, B, and C are functions of x only, that can be determined by collocating the pressure data along $\phi = 0$-, 90-, and 180-deg meridian lines. The pressure gradients are

$$\frac{\partial}{\partial x}\left(\frac{P}{P_0}\right) = \frac{dA}{dx}\cos\phi + \frac{dB}{dx} + \frac{dC}{dx}\cos 2\phi \tag{41}$$

$$\frac{\partial}{\partial \phi}\left(\frac{P}{P_0}\right) = -A\sin\phi - 2C\sin 2\phi \tag{42}$$

Pressure solution by the method of characteristics on $\phi =$ 0-, 90-, and 180-deg meridian lines at $M_\infty = 18$ and $\alpha = 10$ deg are taken from Ref. 19, which were then curve fitted with a polynomial to represent A, B, and C. The theoretical pressure values were used with empiricism built into the interpolation formulas, Eq. (40). A comparison between the interpolated and the original theoretical pressure distributions is shown in Fig. 5.

Equations (40-42), together with body geometry equations and the isentropic relation between the local Mach number and pressure, constitute all the terms needed for the right-hand side of Eq. (21) for calculating streamlines. To start the calculation, the initial conditions are determined by the exact geometrical relations on the spherical cap; see Fig. 6.

$$x_i = \cos^{-1}(\cos\alpha\cos S_i - \sin\alpha\sin S_i\cos\beta)$$

$$\phi_i = \sin^{-1}(\sin S_i\sin\beta/\sin x_i)$$

$$\theta_i = \sin^{-1}(\sin\alpha\sin\beta/\sin x_i) \tag{43}$$

For a spherical body, these exact relations hold everywhere. It is, therefore, convenient to apply these relations right at the juncture and initiate the integration there. The integration of Eqs. (21-23) can be performed accurately using a fourth-order Runge-Kutta scheme to give the location of the streamline in terms of coordinates x and ϕ, and its direction θ measured with respect to the x axis. The calculated streamlines are designated by β values which run from 0 to 180; $\beta = 0$ for the most windward line. The three-dimensional flow separation then can be determined by tracing the envelope of converging inviscid streamlines.

Determination of Flow Separation over a Prolate Spheroid at Incidence

The flow separation over a prolate spheroid (ellipsoid) at specific incidences has been investigated both theoretically[4] and experimentally.[5,6] It is a good case for comparison purposes. Also, since a closed-form potential flow solution is

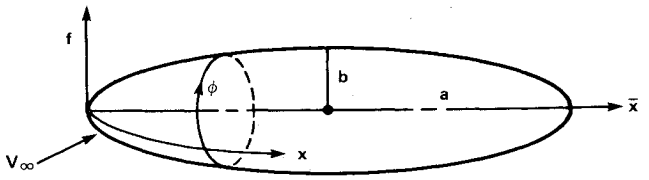

Fig. 7 Geometry of a prolate spheroid.

available for this body, it is convenient to illustrate the viscous procedure proposed earlier.

With the major and minor axes of the ellipsoid defined by a and b, respectively, the body coordinate is given by (see Fig. 7)

$$f=b\sqrt{1-(\bar{x}/a-1)^2} \tag{44}$$

The surface pressure can be expressed by

$$P=P_\infty+\frac{\rho_\infty V_\infty^2}{2}\left(1-\frac{u^2}{V_\infty^2}-\frac{v^2}{V_\infty^2}\right) \tag{45}$$

The required velocity components are given by Wang[21] based on the potential flow solution

$$\frac{u}{V_\infty}=\frac{1}{\left[1-e^2\left(\frac{\bar{x}}{a}-1\right)^2\right]^{1/2}}\left\{(1+k_a)(\cos\alpha)\right.$$

$$\left.\times\left[2\left(\frac{\bar{x}}{a}\right)-\left(\frac{\bar{x}}{a}\right)^2\right]^{1/2}+(b/a)\,(1+k_c)\,(\sin\alpha)\left(\frac{\bar{x}}{a}-1\right)\cos\phi\right\} \tag{46}$$

$$\frac{v}{V_\infty}=(1+k_c)\sin\alpha\sin\phi \tag{47}$$

where α is the incidence and e is the eccentricity given by

$$e=\sqrt{1-(b/a)^2} \tag{48}$$

Parameters k_a and k_c are the axial and cross coefficients of the virtual mass defined by

$$k_a=\left[\frac{1}{2e}\ln\frac{1+e}{1-e}-1\right]\Big/\left[\frac{1}{1-e^2}-\frac{1}{2e}\ln\frac{1+e}{1-e}\right] \tag{49}$$

and

$$k_c=[1/(1+2k_a)] \tag{50}$$

The pressure gradients are readily obtained through the following relations.

$$\frac{\partial P}{\partial x}=-\rho_\infty V_\infty^2\frac{u}{V_\infty}\left[\frac{2\left(\frac{\bar{x}}{a}\right)-\left(\frac{\bar{x}}{a}\right)^2}{1-e^2\left(\frac{\bar{x}}{a}-1\right)^2}\right]^{1/2}\frac{\partial}{\partial\bar{x}}\left(\frac{u}{V_\infty}\right) \tag{51}$$

$$\frac{\partial P}{\partial\phi}=-\rho_\infty V_\infty^2\left[\frac{u}{V_\infty}\frac{\partial}{\partial\phi}\left(\frac{u}{V_\infty}\right)+\frac{v}{V_\infty}\frac{\partial}{\partial\phi}\left(\frac{v}{V_\infty}\right)\right] \tag{52}$$

For this particular case in which the inviscid velocity components are known everywhere, the local inviscid streamline angle θ is also known

$$\theta=\tan^{-1}(v/u) \tag{53}$$

Equation (53) is useful for 1) testing the accuracy of the system, Eqs. (21-23), by comparing the integrated θ value against the exact value and 2) providing the initial condition for calculation of viscous streamlines using Eqs. (30-32).

The viscous streamline equations, Eqs. (30-32), with the aid of Eqs. (44-52) and the proper friction model, can then be integrated using a fourth-order Runge-Kutta scheme. The initial condition for θ is evaluated by Eq. (53) at a point close to the forward stagnation point. Similar to the previous case, the calculated streamlines are designated by β values which run from 0 to 180; $\beta=0$ for the most windward line. The three-dimensional flow separation can then be determined by tracing the convergence of viscous streamlines.

Results and Discussion

The procedure described in the previous section has been coded in FORTRAN using a CDC 6600/6700 computer. Each case, either the spherically blunted cone or the ellipsoid, takes less than 150 statements and occupies a very limited storage. Because of its small size, the program for the ellipsoid case was subsequently converted to the BASIC language using a Tektronix 4051 desk-top computer. The latter has instant graphic capability to facilitate evaluation of the friction model.

Spherically Blunted Cone at $\alpha=10$ deg

The results of a 9-deg spherically blunted cone at $M_\infty=18$ and $\alpha=10$ deg are shown in Fig. 8. All the streamlines are labelled with β values; $\beta=0$ for the most windward line. The streamlines in the upper leeward region turn back to the windside because of flow retardation caused by the empirical nature of the pressure gradient employed. The flow exhibits

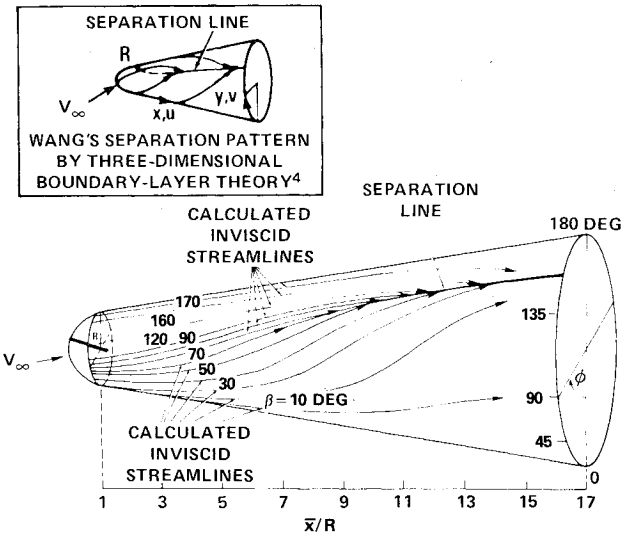

Fig. 8 Separation line over a 9-deg half-angle spherically blunted cone at $M_\infty=18$ and $\alpha=10$ deg.

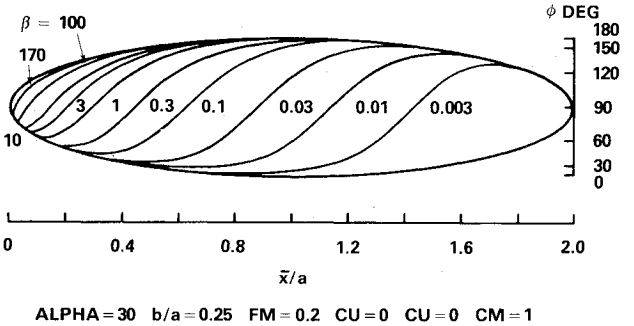

Fig. 9 Inviscid streamlines over a prolate spheroid calculated using potential flow pressure distribution.

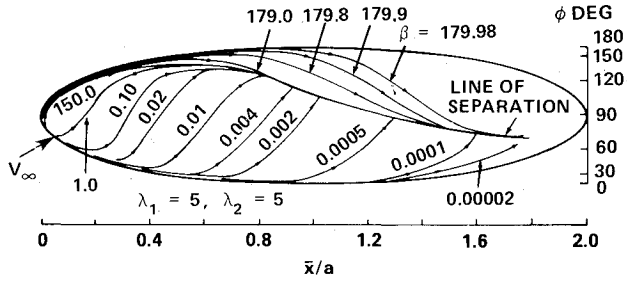

Fig. 10 Line of separation determined by convergence of streamlines over a prolate spheroid ($a/b=4$) at $\alpha=30$ deg.

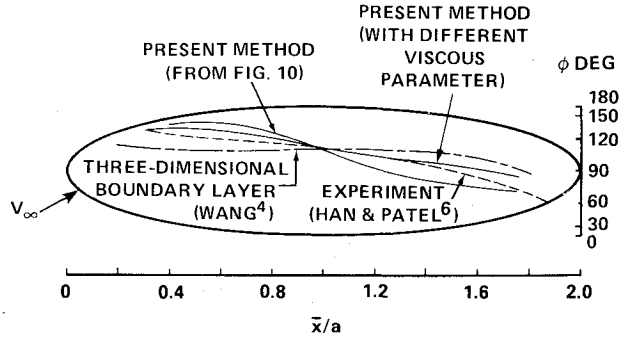

Fig. 11 Comparison of the location of line of separation.

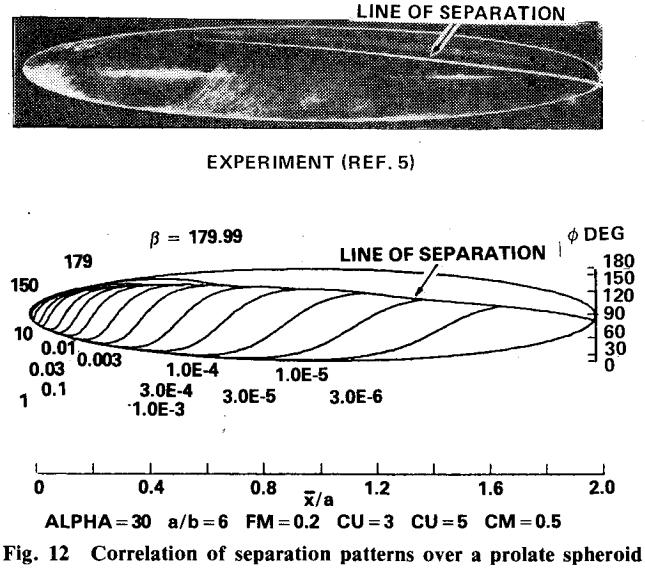

Fig. 12 Correlation of separation patterns over a prolate spheroid ($a/b=6$) at $\alpha=30$ deg.

vortex-layer-type (open type) separation resulting from streamline convergence. The line of separation is easily traced using the envelope concept. A remarkable resemblance between the present result and Fig. 15c of Ref. 4 is observed. This same case was considered by the author earlier.[22] However, then the reason for the leeside streamline bending toward windside was not identified. Consequently, those streamlines for $\beta>90$ deg were not published; see Fig. 12 of Ref. 22.

Prolate Spheroid at Incidences

In the case of a prolate spheroid at incidences in an incompressible flow, both the inviscid approach (streamlines at the edge of boundary layer) and the viscous approach (streamlines inside the boundary layer) were examined numerically.

Using the inviscid approach with pure potential flow pressures, the calculated streamlines monotonically approach the apex of the leeward side; see Fig. 9. The integrated values for the streamline angle θ agree very closely with those exact values given by Eq. (53). It serves as a test case for validating the method.

The viscous approach was first investigated by assigning constant coefficients for the friction model ($\lambda_1=\lambda_2=5$) for the case of a prolate spheroid ($a/b=4$) at $\alpha=30$ deg. The result is depicted in Fig. 10. It indicates that streamlines in the leeward side turn back to the windward side and then encounter those directly from the windward side and, therefore, form a flow separation. The trend is consistent with the previous case. The line of separation is determined by the envelope of converging streamlines. The level of agreement between the present result and the experimental data is comparable to that between the three-dimensional boundary-layer solution and the experiment; see Fig. 11. The results, in general, depend on the magnitude of the damping parameters used. Figure 11 also reveals the effect of the friction model. A slightly improved location of the line of separation can be found as a consequence of changing values of the empirical parameter λ.

Finally, the present viscous result was further compared with recent experimental data provided by Kreplin et al.[5] Empirical constants for the friction model were adjusted so that the theoretically determined separation pattern matched that of the experimental one. This is depicted in Fig. 12 for an $a/b=6$ prolate spheroid at $\alpha=30$ deg. The constants were found as follows

$$a_1=3.0 \quad b_1=5.0, \quad a_2=5.0 \quad b_2=-3.6$$

for Eqs. (36) and (37). The set represents one of many possible combinations. In general, the parameter λ is affected by the nature of the boundary layer, the compressibility, the velocity profile, and, possibly, the angle of attack. The first three may be represented by the Reynolds number, the Mach number, and the pressure gradient. A physically oriented friction model is yet to be developed in the future.

Concluding Remarks

A streamline approach for determining the free vortex-layer-type, three-dimensional flow separation has been developed. Both inviscid and viscous approaches were considered. For the inviscid method, the more realistic are the input surface pressures, the more realistic are the streamline and, therefore, the separation patterns. Experimental or empirical pressure distributions or theoretical pressures, obtained by means of viscous-inviscid distributions or theoretical pressures, are considered to possess such physical properties.

The viscous approach allows use of pure inviscid pressures along with proper viscous damping. The accuracy of the new, simple method depends on the ability of modeling the frictional force in the boundary layer. An approximate model based on the equality condition between the frictional and inertial forces works reasonably well for the case of a prolate spheroid at incidence. The model needs to be improved with more considerations from a boundary-layer point of view.

Nevertheless, because of its simplicity and small computation requirement, the present approach may become a useful tool to facilitate computation of viscous-inviscid interactions with flow separation in three dimensions and to predict the interference drag involving free vortices resulting from flow separation.

Acknowledgments

This research was sponsored by the Naval Air Systems Command (AIR-320D, AIRTASK 9R023-02) under the cognizance of D. Kirkpatrick. The author is indebted to F. R. DeJarnette of North Carolina State University; K. C. Wang

of San Diego State University; S. de los Santos, M. Martin, and H. J. Lugt of DTNSRDC for their useful discussions and comments; and to D. G. Rousseau for his assistance in computer programming. Thanks are also due to G. Schneider of DFVLR, West Germany, and the anonymous reviewer who have kindly pointed out some errors in the preprint.

References

[1] Eichelbrenner, E. A. and Oudart, A., "Methods de Calcul de la Couche Limite Tridimensionelle. Application a un Corps Fusele Incline sur le Vent," ONERA Publ. 76, Chatillon, France, 1955.

[2] Maskell, E. C., "Flow Separation in Three Dimensions," Royal Aircraft Establishment, Bedford, England, RAE Rept. Aero 2565, Nov. 1955.

[3] Wang, K. C., "Separation Patterns of Boundary Layers over an Inclined Body of Revolution," *AIAA Journal*, Vol. 10, Aug. 1972, pp. 1044-1050.

[4] Wang, K. C., "Separation of Three-Dimensional Flow," Martin Marietta, Baltimore, Md., MML TR-76-54C, Aug. 1976.

[5] Kreplin, H. P., Vollmers, H., and Meier, H. U., "Experimental Determination of Wall Shear Stress Vectors on an Inclined Prolate Spheroid," presented at the 5th U.S.-West Germany Data Exchange Agreement Meeting on Viscous and Interacting Flow Field Effects, Annapolis, Md., April 1980.

[6] Han, T. and Patel, V. C., "Flow Separation on a Spheroid at Incidence," *Journal of Fluid Mechanics*, Vol. 92, Pt. 4, 1979, pp. 643-657.

[7] Stetson, K. F. and Friberg, E. G., "Surface Conditions in the Leeward Region of a Blunt Cone at Angle of Attack in Hypersonic Flow," Aerospace Research Lab, Wright-Patterson Air Force Base, Dayton, Ohio, ARL-69-0114, July 1969.

[8] Nielsen, J. N., "Missile Aerodynamics—Past, Present, Future," AIAA Paper 79-1819, presented as Wright Brothers Lectureship in Aeronautics at AIAA Aircraft Systems and Technology Meeting, New York, N.Y., Aug. 1979.

[9] Peake, D. J. and Tobak, M., "Three-Dimensional Interactions and Vertical Flows with Emphasis on High Speeds," AGARDograph 252, July 1980.

[10] Grosche, F. R., "Wind Tunnel Investigation of the Vortex System Near an Inclined Body of Revolution with and without Wings," AGARD CP-71, 1970.

[11] Tanaka, H. and Ueda, T., "Study on the Structure of Ship Vortices Generated by Full Sterns," *Proceedings of 12th Symposium on Naval Hydrodynamics*, Washington, D.C., June 1978.

[12] Rosenhead, L., ed., *Laminar Boundary Layers*, Oxford University Press, Oxford, England, 1963, pp. 488-491.

[13] Harris, E. L., "Determination of Streamlines on a Sphere-Cone at Angles of Attack from the Measured Surface Pressure Distribution," Naval Ordnance Laboratory, Silver Spring, Md., Rept. NOL TR-63-37, Feb. 1963.

[14] Maikapar, G. I., "Calculation of Streamlines with a Known Pressure Distribution on the Surface of a Rigid Body," *Journal of Applied Mathematics and Mechanics*, Jan. 1965, pp. 468-470.

[15] DeJarnette, F. R., "Calculation of Inviscid Surface Streamlines and Heat Transfer on Shuttle Type Configurations," NASA CR-111921, Aug. 1971.

[16] Rakich, J. V. and Lanfranco, M. J., "Numerical Computation of Space Shuttle Laminar Heating and Surface Streamlines," *Journal of Spacecraft and Rockets*, Vol. 14, May 1977, pp. 265-272.

[17] Tai, T. C., "Determination of Streamline Geometry and Equivalent Radius over Arbitrary Bodies with Application to Three-Dimensional Drag Problem," David Taylor Naval Ship Research and Development Center, Bethesda, Md., DTNSRDC-79/080, Dec. 1979.

[18] Schlichting, H., *Boundary Layer Theory*, 4th English Ed., McGraw-Hill, New York, 1960, pp. 25, 113-114.

[19] Knox, E. C. and Lewis, C. H., "A Comparison of Experimental and Theoretically Predicted Pressure Distributions and Force and Stability Coefficients for a Spherically Blunted Cone at $M_\infty = 18$ and Angle of Attack," ARO, Inc., AEDC-TR-65-234, Feb. 1966.

[20] Zakkay, V., "Pressure and Laminar Heat Transfer Results in Three-Dimensional Hypersonic Flow," WADC TN 58-182, ASTIA Doc. AD 155-679, Sept. 1958.

[21] Wang, K. C., "Boundary Layer over a Blunt Body at High Incidence with an Open-Type Separation," *Proceedings of the Royal Society of London, Series A*, Vol. 340, 1974, pp. 33-55.

[22] Tai, T. C., "Laminar and Turbulent Convective Heat Transfer Over Bodies at an Angle of Attack," Ph.D. Thesis, Virginia Polytechnic Institute, Blacksburg, Va., Oct. 1968.